Caving 2026 – A van As, D Cumming-Potvin & J Wesseloo (eds)

doi:10.36487/ACG_repo/2645_94

Calibration of caving behaviour in Macroblock S2S3 at Chuquicamata underground mine using 3D numerical modelling

Catalina Álvarez [a,*], Claudio Barra [a], Giuseppe Barindelli Pizarro [b]

[a] *ITASCA, Chile*

[b] *Chuquicamata Division, Codelco, Chile*

Abstract

The transition of the Chuquicamata mine in Chile to large-scale block caving has required a robust understanding of rock mass response and cave propagation mechanisms at depth. The mine was designed with multiple macroblocks, with operations starting in the central macroblock in 2019. Caving performance has been strongly influenced by orebody heterogeneity, leading to local challenges in the southern sector of the central macroblock. Caving in Macroblock S2S3 stalled, requiring mitigation measures that involved blasting the pillar between S2S3 and the adjacent central macroblock, which ultimately triggered cave propagation.

This study presents the calibration of caving behaviour for Macroblock S2S3 using 3D numerical modelling based on a hybrid approach combining FLAC3D and MassFlow (gravity flow) software. Key calibration parameters are related to post-peak rock mass behaviour. Geological and geotechnical inputs were kept unchanged, reflecting a robust site characterisation through a rock mass rating block model (GSI). A key outcome of the calibration is the reproduction of cave breakout, including its size and location, as identified by the monitoring system and captured by the numerical model. The calibration improved the reliability of numerical predictions and provided a sound basis for future analyses. Modelling results for predictive mining are presented as an application.

Keywords: *block caving, Chuquicamata mine, preconditioning, gravity flow, FLAC3D*

1 Introduction

Chuquicamata underground mine is one of the most significant large-scale cave mining transitions in the industry. Production started in May 2019 with undercutting of the central macroblock (N1S1) of the first lift, located approximately 200 m below the open pit floor. In heterogeneous orebodies, unforeseen structural or rock mass conditions can delay propagation even when extraction is progressing according to plan. In the southern sector of the central production area, this challenge became apparent when Macroblock S2S3 failed to propagate after start-up and responded only after the pillar towards the central macroblock was partially blasted. That sequence of events created an unusually valuable calibration opportunity because it encompassed both a stalled and a triggered cave state within the same broad geotechnical setting.

The core technical problem addressed in this paper is therefore not simply whether caving occurs, but whether a numerical framework can reproduce the transition from non-caving to caving for the correct mechanical reasons and then transfer that calibration to future mining sectors. This distinction is not academic. If a model is calibrated by arbitrarily weakening the rock mass, it may reproduce timing while obscuring the actual controls on propagation. By contrast, if the geological and geotechnical

* Corresponding author. Email address: catalina.alvarez@oneitasca.com

characterisations are preserved and calibration is achieved through post-peak behaviour, the resulting model is more defensible when applied to different footprints, preconditioning layouts and extraction sequences.

The study combines FLAC3D (ITASCA 2023) and MassFlow (ITASCA 2025) software in a coupled workflow. FLAC3D resolves the evolving stress deformation response and damage state of the rock mass, while MassFlow resolves the gravity flow, rilling, cavity geometry and airgap development associated with the draw. This coupling methodology is illustrated in Figure 1.

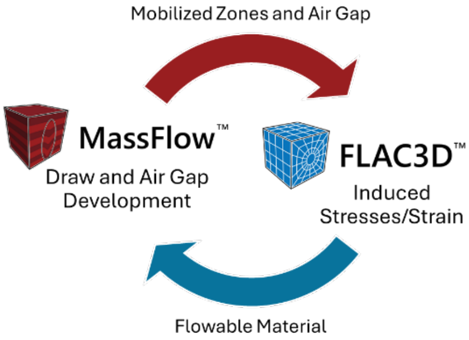

Figure 1 Schematic description of the numerical coupling

The coupling is particularly important in cave mining because operational risk is strongly influenced by void geometry and by the persistence of unfilled cavities; features that are difficult to reproduce with continuum-only cave models. The method is calibrated against the observed S2S3 response and then applied predictively to macroblocks N41 and N42, for which the mine required practical guidance on aspects of preconditioning and sequencing. Figure 2 illustrates a schematic view of the first lift location, along with the relative locations of the macroblocks relevant to the analyses.

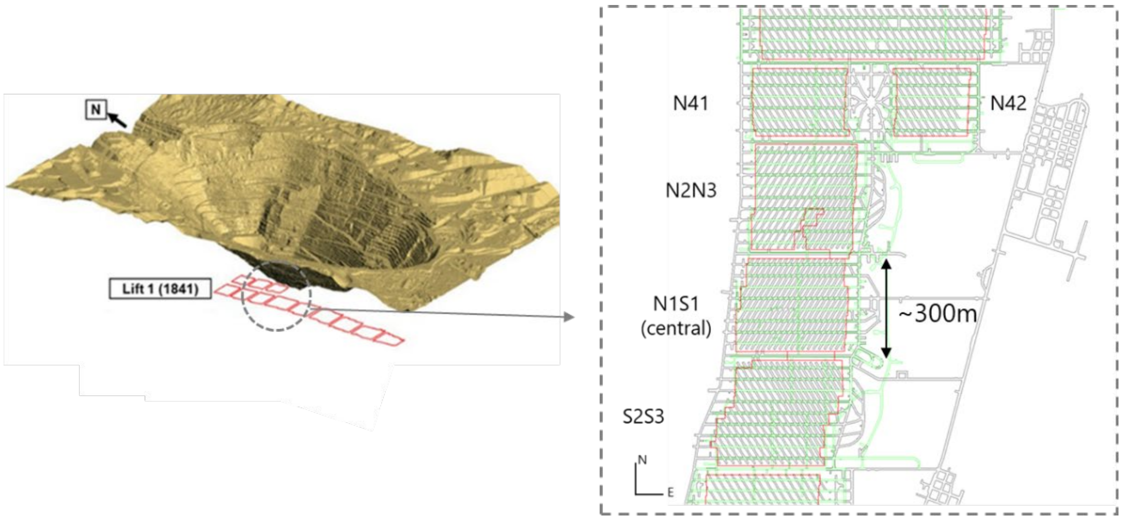

Figure 2 Lift 1 layout with a close-up showing macroblocks of interest

The objectives of the work are fourfold: firstly, to calibrate a coupled FLAC3D–MassFlow model against the observed behaviour of Macroblock S2S3; secondly, to verify whether the model reproduces the timing, location and geometry of cave breakout captured by surface monitoring; thirdly, to apply the calibrated post-peak response to predictive assessments of macroblocks N41 and N42; and fourthly, to quantify the effects of preconditioning and mining sequence on cave initiation, cavity regularity, airgap development, surface connection and propagation rate. The value added for the caving community lies in the combination of full-scale back-analysis coupled with mechanical flow representation and decision-ready thresholds expressed in terms of hydraulic radius, incorporated area and cave-rise efficiency.

2 Geotechnical data

The Chuquicamata porphyry deposit is composed mainly of 3 units defined according to different degrees of alteration and mineralisation. The units are known as PEK (potassic), PES (sericitic) and RQS (quartz sericitic). The latter, depending on the RQS content, is further divided into QIS (Q = S), QMES (Q < S) and QMS (Q > S). The rock mass strength properties are described in terms of standard rock mass parameters (density, σ_{ci}, GSI, and m_i). Peak intact inputs were taken from site characterisation while GSI was imported spatially from block models rather than imposed as a single average value. The material parameters depend on the macroblock location as defined in Table 1.

The structural model for the underground mine contains 146 faults as shown Figure 3. Local filtering retained 70 structures for the S2S3 calibration model and 68 structures for the N41-N42 predictive model. These structures were implemented explicitly in FLAC3D as zone joints. Fault strengths vary with friction between 25–30° and cohesion between 40–50 kPa, except for the regional structure known as the West Fault, which is characterised by 18° friction and 20 kPa cohesion.

The stress regime corresponds to an induced stress environment caused by the open pit (approximately 1,000 m deep). The pit bottom is approximately 200 m above lift-1. The underground mine represents a low-stress environment with good to fair rock mass quality, which is quite different from the high-stress environment of Chile's El Teniente mine, also owned by CODELCO.

Table 1 Relevant peak material properties used in the local models. The Geological Strength Index was spatially variable and imported from block models

Macroblock	Unit	Density (kg/m^3)	σ_{ci} (MPa)	E_i (GPa)	m_i
S2-S3	PEK	2,620	83	50	28
S2-S3	PES	2,660	66	30	16
S2-S3	QIS	2,700	58	30	17
S2-S3	QMS	2,720	68	51	13
N41-42	PEK	2,619	94	57	15
N41-42	PES	2,610	72	41	17
N41-42	QIS	2,711	71	30	22
N41-42	QMS	2,718	74	39	8

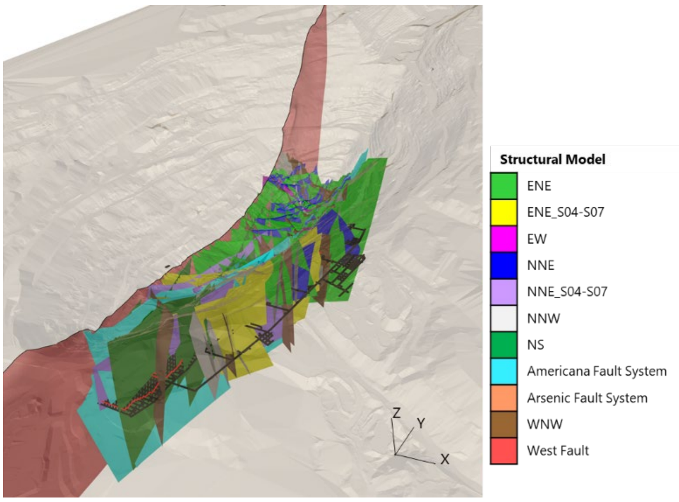

Figure 3 Structural model for Chuquicamata underground mine

3 Numerical modelling framework

3.1 Local scale models

The analyses are developed within local model frameworks and consider stress initialisation states obtained from an open pit mine scale stress model. The stresses in the larger model are first installed for a pre-mining state (coming from a stress calibration analysis), and then the induced stresses are tenses obtained after excavating the pit. They represent the initial condition for the underground analyses. Note that Chuquicamata has developed an extensive database of stress measurements, enabling stress calibration analyses for the site. The local models also include neighbouring active macroblocks as boundary conditions so that cave interaction is not ignored. The model for S2-S3 analysis is depicted in Figure 4 and that for N41-42 in Figure 5. The pre-mining stress condition for N41-N42 is given in Figure 6, which shows the influence of the nearby active macroblocks (as N2-N3).

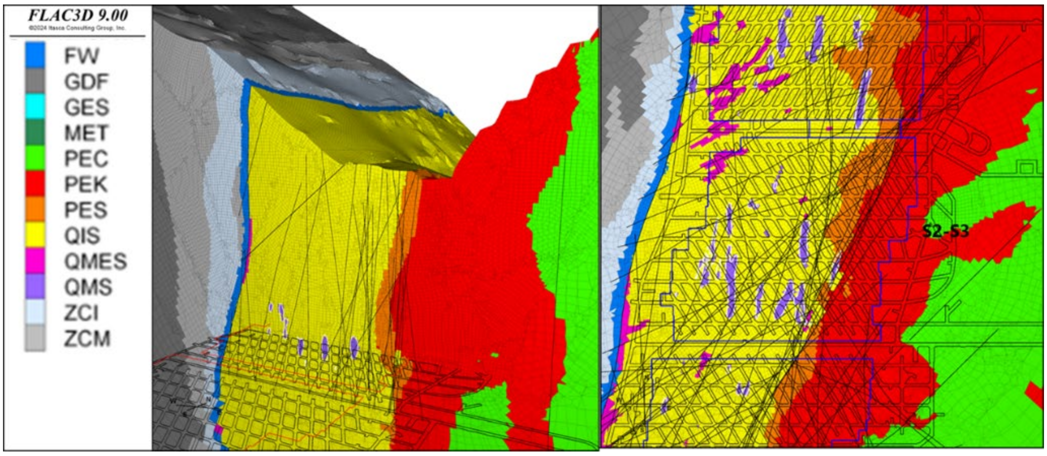

Figure 4 Local FLAC3D model for S2-S3 analysis

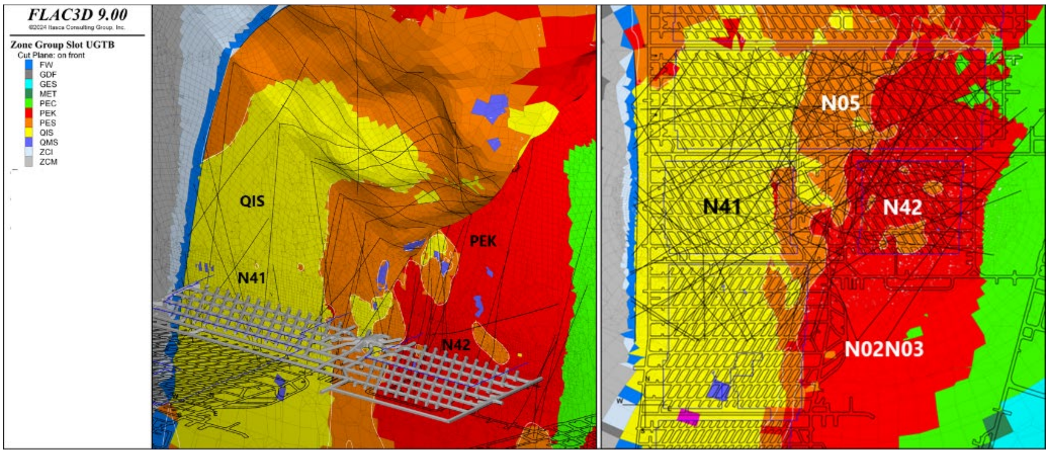

Figure 5 Local FLAC3D model for N41-42 analysis

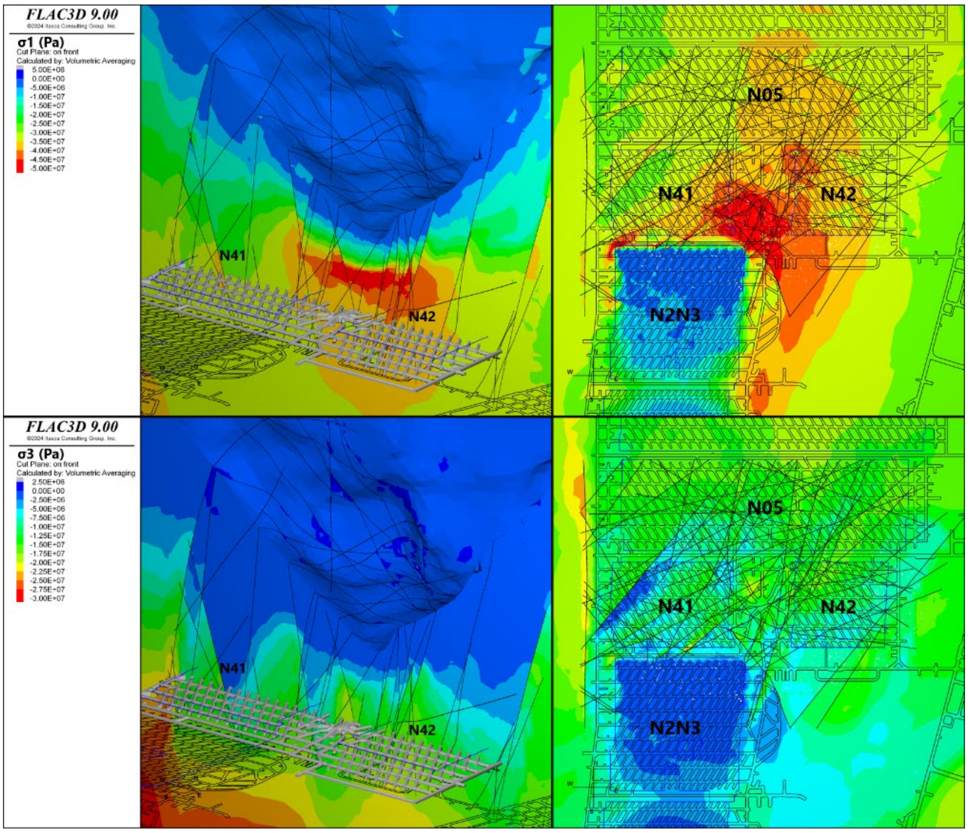

Figure 6 (a) N41-N42 pre-mining stress conditions showing major principal components; (b) Minor principal components (compress stress is negative)

3.2 Constitutive model and cave-flow coupling

Mechanical response was simulated in FLAC3D using the Itasca Model for Advanced Strain Softening (IMASS), which reproduces cohesion weakening, tensile strength loss, frictional strengthening, modulus softening, density adjustment and bulking-related dilatancy. The Hoek–Brown failure surface was defined using the site-specific parameters sigma_c_i, m_i and GSI, with disturbance factor (D) of D = 0 (Hoek et al. 2002). The rock mass stress–strain behaviour is illustrated in Figure 7, showing the post-peak response which is driven by the critical strain, defined by default using Equation 1 (Lorig & Pierce 2000), where 'd' denotes the model zone size. The ultimate strength is driven by volumetric deformation (bulking).

The principal calibration variable is the plastic shear strain, which is adjusted by a multiplier (μ)controlling the brittleness or ductility of post-peak behaviour (Lorig & Pierce 2000). Values of μ below 1.0 impose a more brittle response, while values above 1.0 impose a more ductile response. The S2S3 back-analysis showed that the default value (μ = 1.0), combined with an appropriate flowability threshold, was sufficient to reproduce the observed non-caving state prior to pillar blasting.

The IMASS state variable strength loss (sloss) depicted in Figure 7 was used as a direct indicator of degradation, ranging conceptually from peak behaviour (approximately +1) through post-peak (approximately 0) towards residual strength (approximately −1). This variable is central to the coupled methodology because it links mechanical degradation in FLAC3D to material availability in MassFlow (see Figure 1). A zone was considered available to flow only when either 1 of 2 conditions was met: vertical settlement greater than 1 m or sloss < −0.01. The displacement threshold is consistent with comparable caving practice whereas the sloss threshold is mine-specific and was derived from the S2S3 calibration.

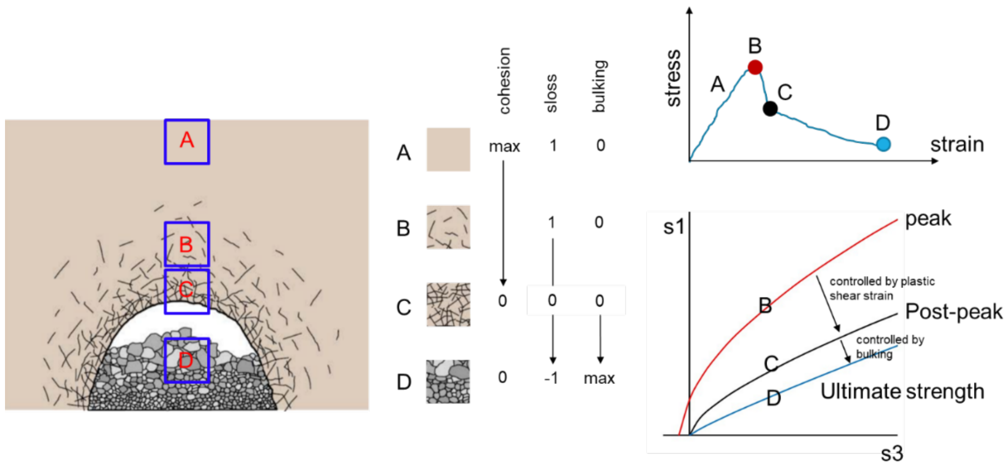

Figure 7 Schematic representation correlating various degrees of damage in a rock mass with post-peak behaviour (points B, C and D) (Ghazvinian et al. 2020)

$$\varepsilon^{p}_{crit} = (12.5–0.125\ GSI)/100d \quad (1)$$

MassFlow simulated 3D gravity flow, cave geometry, rilling and airgap development under the imposed draw schedule (Lorig & Cundall 2000; Pierce 2010). Input assumptions included a regular primary fragmentation distribution defined by a Weibull curve, zero initial porosity, maximum porosity of 30%, bulk density of 2.7 t/m^3 and a fragmented material friction angle of 38˚. Although the primary fragmentation was not varied spatially, the coupled framework still captured a more realistic cave geometry than continuum-only approaches because flow is conditioned by the evolving mechanically available volume rather than by an imposed geometrical rule.

The advance of mining is defined by the cavity generated by the markers in MassFlow, as illustrated in Figure 8. These markers represent the air pocket (red), the areas mobilised by the extraction process (yellow) and by the rilling mechanism (brown). As the cavity advances and breaks through the surface, the air will form a crater.

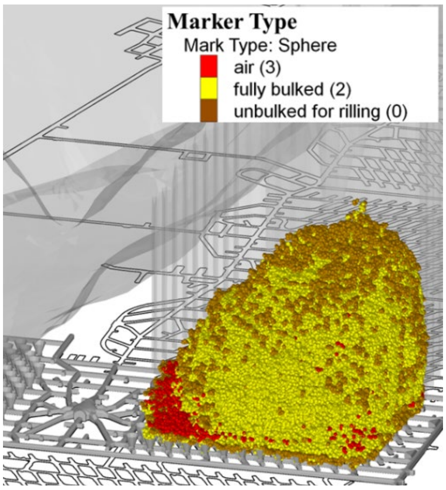

Figure 8 Definition of cavity advancement based on the type of marker in MassFlow

4 Calibration of Macroblock S2S3 behaviour

Calibration targeted the period from October 2021 to October 2022 in S2S3. Two milestones had to be reproduced. The first was a non-caving condition during sustained extraction before the pillar was blasted. The blasting involved long-range holes approximately 30 m long. The second was activating caving after partial blasting of the pillar between S2S3 and the central macroblock. The blasting campaign progressed in May, July and September 2022 as shown in Figure 9. In the model, the blasted pillar was represented as broken material at IMASS residual strength, with zero initial stresses, consistent with its role as a low-confinement pathway to a pre-existing cave void.

This set-up is important because it allows the calibration to distinguish between two possible mechanisms for delayed caving. One possibility is that the S2S3 rock mass was simply too strong to cave under the imposed extraction history. The other is that the column could cave, but only once a permissive boundary condition developed towards the neighbouring void. The model results support the second interpretation: the cave did not need a wholesale reduction in rock mass strength but rather a realistic description of post-peak degradation and confinement relief.

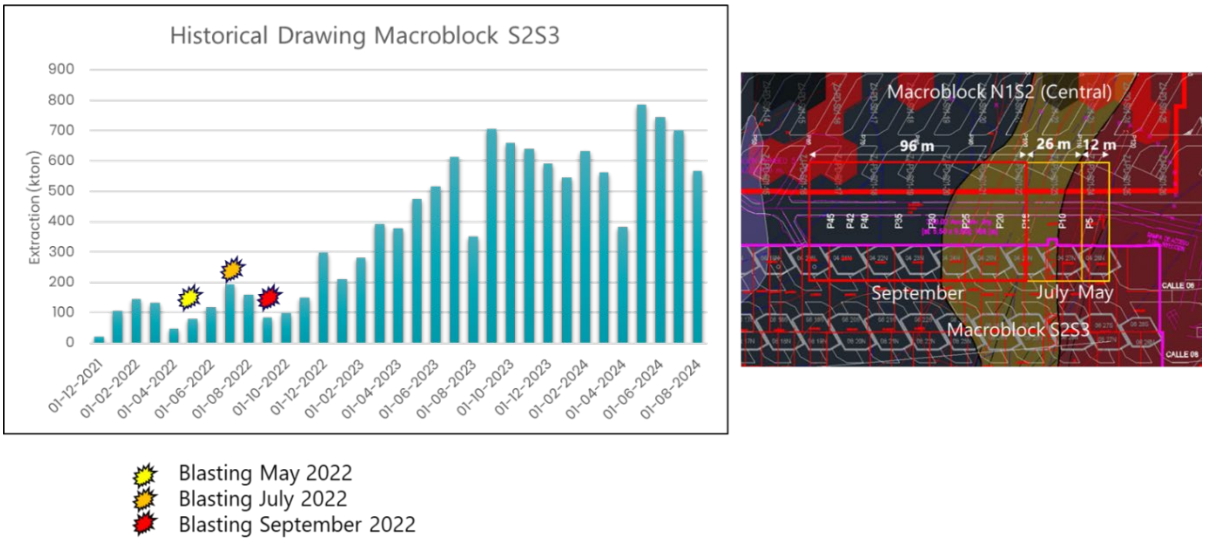

Figure 9 Historical extraction of S2S3, with geometry and the timing of blasting in the pillar against the central macroblock

The most important result of the calibration exercise is that S2S3 non-propagation was reproduced without modifying the geological model or imposing arbitrary strength reductions. Using $\mu=1.0$ and the coupled flowability criterion described in Section 3.2, the model maintained a non-caving configuration through October 2022, indicating that the existing site characterisation was already sufficient to explain the observed behaviour once post-peak degradation was represented appropriately. This is a technically meaningful result. In many cave studies, calibration is obtained by reducing strength until caving occurs. That can match timing, but it also weakens the transferability of the model because the final calibration may no longer preserve the true mine characterisation. In the present case, the calibrated behaviour emerged from a physically interpretable post-peak response rather than from a redefinition of the rock mass itself.

After the pillar was blasted, the model produced rapid propagation toward the west, where QIS and the neighbouring central cave created a lower confinement path. Propagation into the more competent PES sector was significantly less developed over the same period. This asymmetry is mechanically credible and suggests that the model was not merely responding to the artificial insertion of broken material (pillar blasting) but to the interaction between material competence, available void space and stress relief. Operationally, the implication is that the pillar blasting did more than provide fragmented material. It changed the boundary condition of the cave column by connecting S2S3 to a mechanically permissive environment adjacent to the central macroblock.

Comparison with surface displacement monitoring showed reasonable agreement in the mobilised area and the location of breakout. The model also reproduced the practical importance of the damaged band at the pit floor, approximately 60 m thick, implying that once the cave rises into that zone, surface manifestation can occur rapidly. A summary of the model outcome and comparison with surface monitoring data prior to pillar blasting (before September 2022) is provided in Figure 10, and for afterwards in Figure 11.

During the pre-connection stage, seismic activity was concentrated ahead of the caving front (northwestern sector) and below the 1,900 m elevation, with few events occurring around faults located in the central and eastern portions of the macroblock. Thus, seismic data was not useful in defining the evolving cave boundary, with surface movement location being the most relevant data.

The S2S3 calibration is therefore not just a back-analysis success. It establishes a robust basis for predictive modelling by showing that the coupled framework can reproduce both a stalled state and a triggered state under the same geotechnical characterisation. This is an important innovation because problematic caves are often recalibrated retrospectively in ways that cannot be transferred confidently to new sectors.

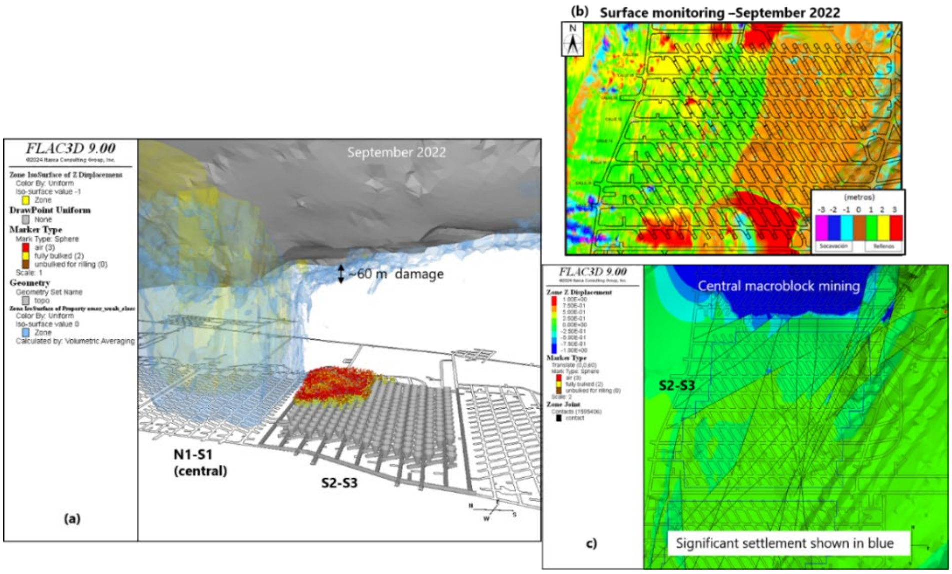

Figure 10 (a) Calibrated S2S3 cave geometry before pillar blasting; (b) With surface monitoring; (c) Model surface settlement

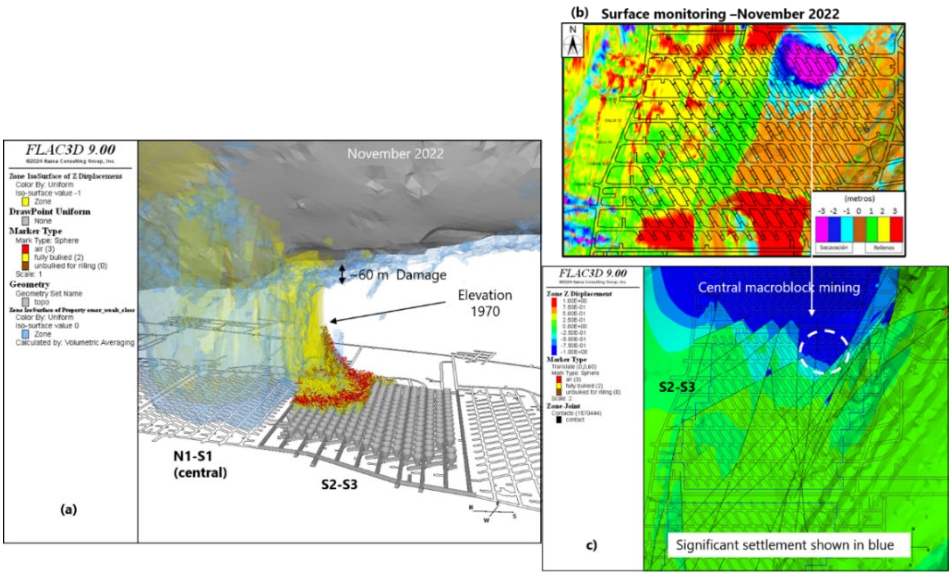

Figure 11 (a) Calibrated S2S3 cave geometry after pillar blasting; (b) Surface monitoring; (c) Model surface settlement

5 Predictive analyses for macroblocks N41 and N42

N42 presents a clearly more adverse caveability condition than N41 because much of the macroblock lies within PEK, which is more competent than QIS (see Figure 5). The analysis cases were focused on N42 due to the forecast cave stalling conditions. Three predictive cases were analysed for N41-N42. The base case used sequence 01 with no preconditioning in N42. The second case retained sequence 01 but added preconditioning in N42. The third case retained preconditioning and changed only the N42 mining direction from east to west to west to east. N41 was not preconditioned in any case. The 2 sequences are described in Figure 12. The preconditioning is illustrated in Figure 13. This structure isolates the main operational levers: firstly, the effect of preconditioning under a fixed extraction sequence and then the effect of a sequence under a fixed preconditioning design.

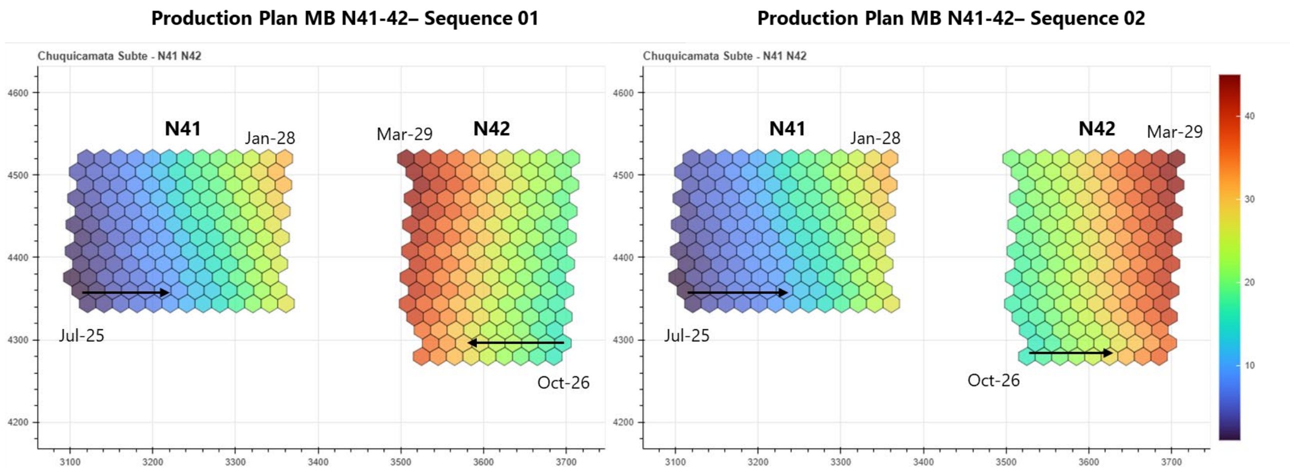

Figure 12 Details of undercutting Macroblock 41-42 (colours represent the number of months after the start of production) for 2 alternative sequences

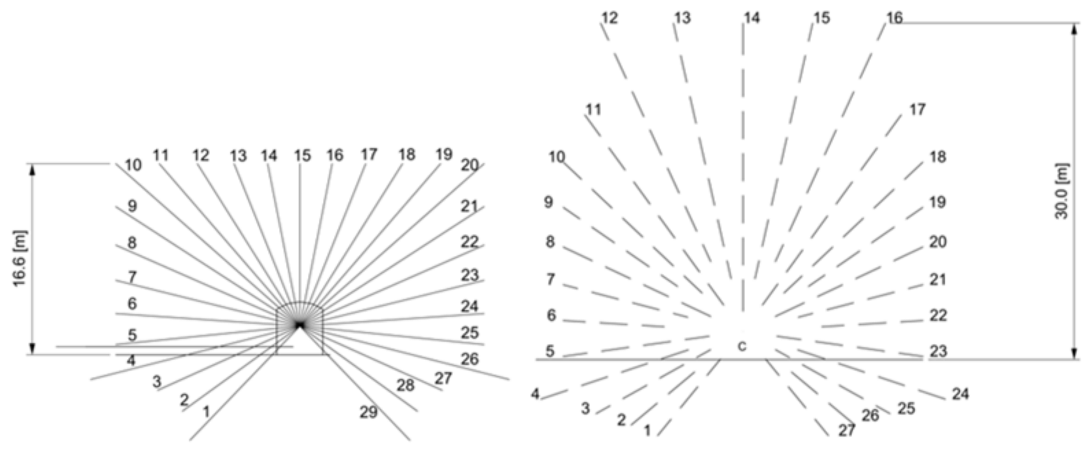

(a) (b)

Figure 13 (a) Blasting design for undercut level defining standard design; (b) Preconditioning design for N42

5.1 Predictive response of Macroblock N42: base case versus preconditioning

In the base case, N42 production begins in October 2026, but cave initiation does not occur until January 2028. By that stage, 67% of the footprint has been incorporated, corresponding to a hydraulic radius of about 43.3 m. Prior to surface connection, the model predicts a more irregular cavity with larger air pockets at the shoulders and apex. This distinction matters. From an operational standpoint, persistent airgaps are not neutral features. They increase the likelihood of delayed collapses, can disrupt the regularity of cave growth and complicate the interpretation of cave maturity from production data. One of the major benefits of the coupled FLAC3D–MassFlow methodology is precisely that it makes these features visible in the analysis rather than hiding them behind a simplified cave shell. The result comparisons with the preconditioning case are given in Figures 14 and 15.

Adding preconditioning under the same extraction sequence materially improves the N42 response by improving cave initiation to November 2027, corresponding to 61% of the incorporated footprint and a hydraulic radius of about 40.4 m. The numerical reduction in threshold is significant but the improvement in cavity regularity may be even more valuable. Preconditioning produces a cleaner, more uniform cave with less persistent air at the crown and margins. It facilitates a more coherent cave column, thereby reducing the duration over which hazardous or production-limiting airgaps remain suspended in the system.

A useful way to interpret the preconditioning benefit is to view it as a reduction in the cave initiation threshold rather than as a binary change from non-caving to caving. In the base case, N42 requires nearly two-thirds of the footprint to be active before propagation occurs. With preconditioning, that threshold falls to roughly three-fifths and R_H decreases from about 43.3 to 40.4 m. That framing is more useful for design and scheduling than a simple statement that preconditioning is beneficial. It converts preconditioning into a quantifiable shift in caveability criteria that planners can compare directly against the achievable monthly incorporation of area.

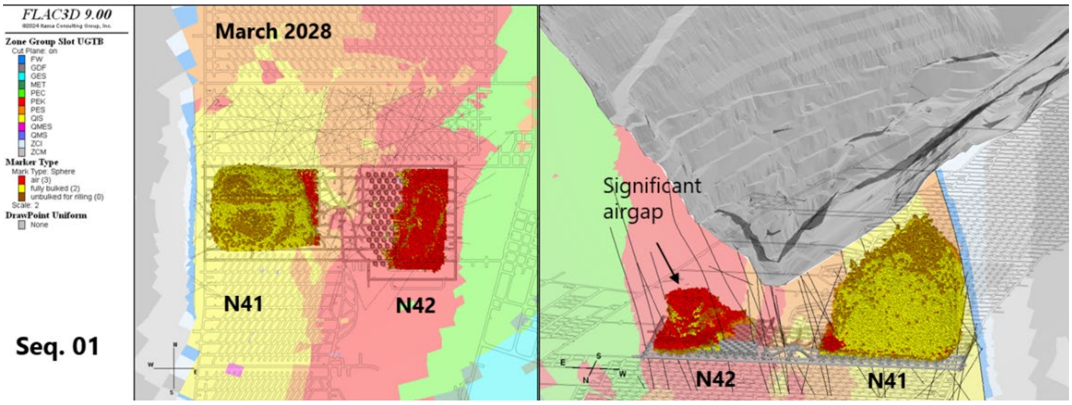

(a)

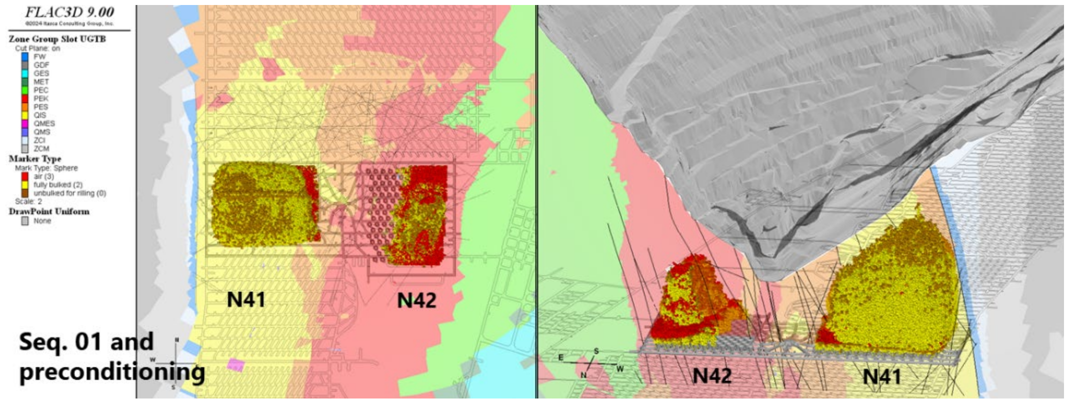

(b)

Figure 14 Comparison of N42 cavity development for Sequence 01: (a) Without preconditioning; (b) With preconditioning

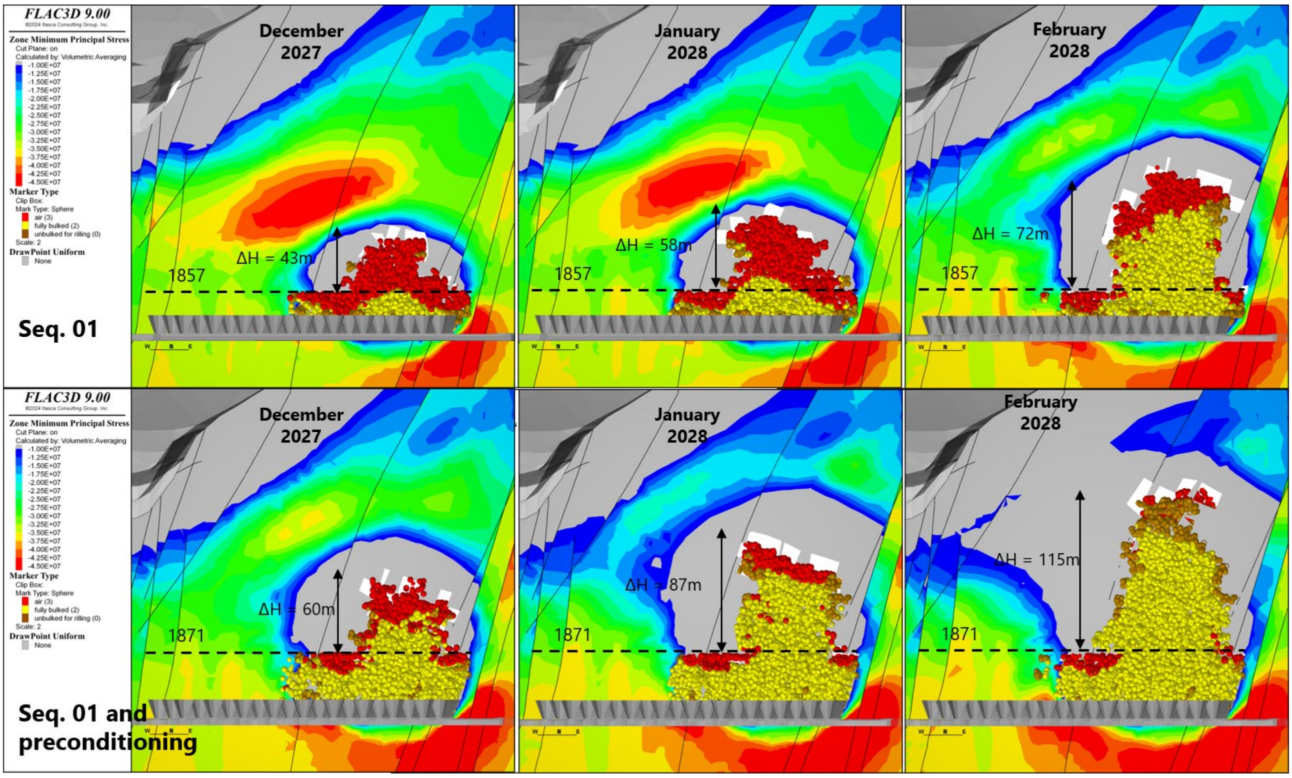

Figure 15 Major principal stress contours overlaying cave geometry for selected periods

5.2 Effect of mining sequence in N42

When preconditioning is retained, and only the mining direction is changed, the model predicts a further improvement in N42 caveability. Under sequence 02, in which mining advances from west to east, N42 initiates in September 2027 after approximately 55.0% of the footprint has been incorporated. The corresponding hydraulic radius is about 36.3 m. Surface connection is advanced by 6 months to March 2028, which is 6 months earlier than sequence 01 and 7 months earlier than the base case.

The mechanical interpretation is consistent with the mine geometry. The western side of N42 lies closer to the open pit and is therefore subject to a more deconfined stress environment. By attacking the macroblock from west to east, the sequence mobilises the most mechanically accessible part of the footprint earlier and allows the cave to rise from a lower confinement boundary condition. The model also predicts more pronounced spill or ravelling propagation on the eastern pit wall under this sequence because the cavity daylights earlier and closer to the pit floor.

The sequence result is one of the strongest practical outcomes of the study. The order in which the footprint is activated matters. In N42, the sequence effect is not a second-order refinement. It reduces the cave initiation threshold from 61% area and R_H of about 40.4 m to 55% area and R_H of about 36.3 m in sequence 02. Put differently, the same preconditioning design becomes significantly more effective when paired with the sequence that engages the less confined sector first.

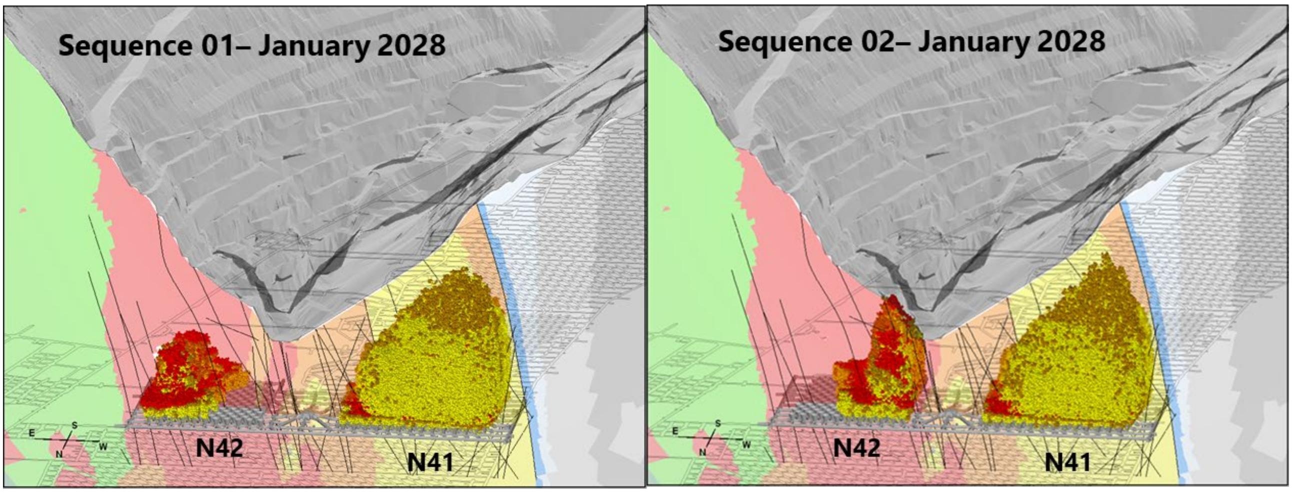

Figure 16 Comparison of N42 cavity development for sequences 01 and 02 (both with preconditioning in N42)

5.3 Propagation rates and cave-rise efficiency

The study also evaluated propagation rates, defined as the ratio of the fractured column height measured from the cave floor to the extraction height. This metric is useful because it normalises cave-rise against production progress and therefore provides a more direct measure of cave efficiency than cavity height alone. For N41 the propagation rate was 5:1 by January 2027, before surface connection as shown in Figure 17 .

In the case of N42, Figure 18 shows the propagation rate comparison for sequence 01 with and without preconditioning at a similar period, showing an increase from 3:1 to 4:1. This indicates that preconditioning makes the N42 cave column more responsive per unit of extraction height, which is consistent with the lower initiation threshold and the more regular cavity shape described previously.

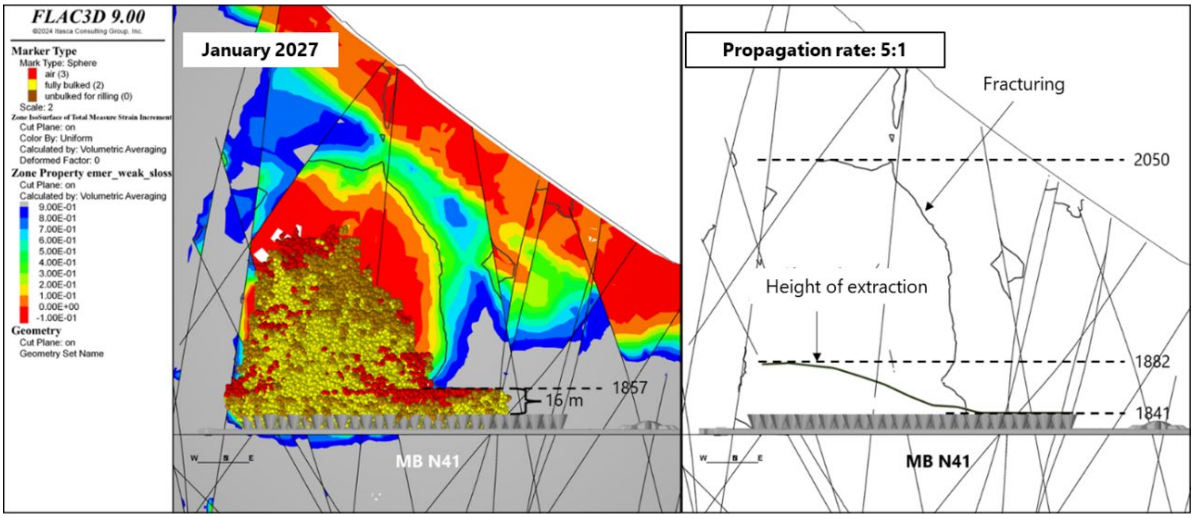

Figure 17 Section view illustrating the evaluation of the propagation rate for N41

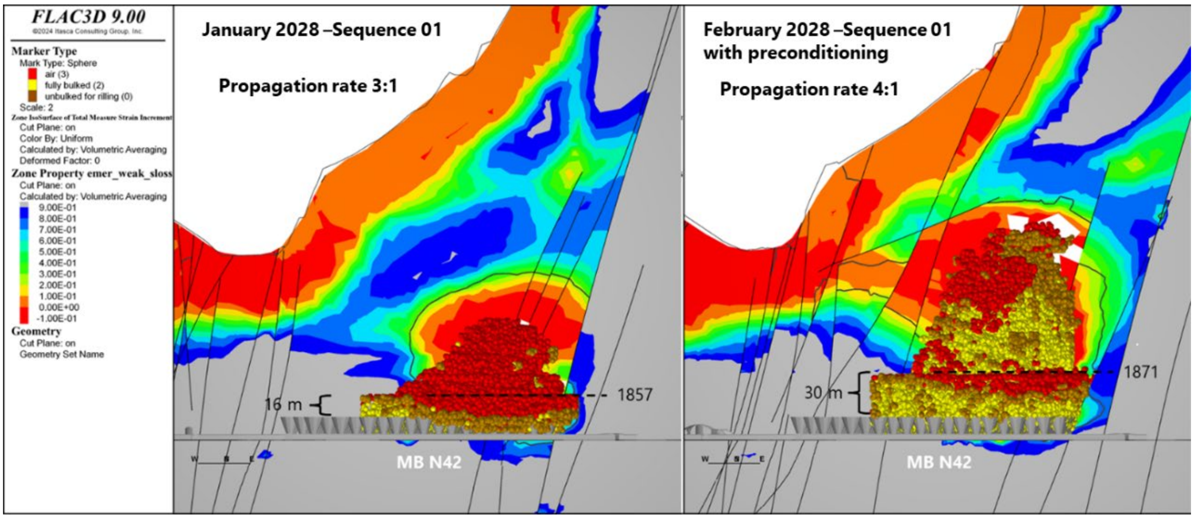

Figure 18 Section view illustrating cave geometry and the propagation rate for N42 for sequence 01 without and with preconditioning at a similar period

6 Conclusion

The coupled FLAC3D-MassFlow methodology successfully reproduced the observed behaviour of Macroblock S2S3 without changing the geotechnical characterisation. The key calibration outcome was obtained by preserving the site characterisation and calibrating post-peak behaviour through the Itasca Model for Advanced Strain Softening critical strain framework. Reproducing both the stalled and triggered states with the same geotechnical characterisation gives confidence that the governing mechanism was captured rather than imposed.

The predictive analyses for N41-42 represent a suite of design-related options, such as preconditioning and sequence alternatives, linked to measurable shifts in caveability thresholds. For N42, preconditioning reduces the initiation requirement from about 67 to 61% of the footprint and lowers R_H from about 43.3 to 40.4 m. Reversing the sequence with preconditioning lowers the threshold further to 55% and R_H about 36.3 m. These are decision-ready outputs. They allow planners to compare a proposed extraction schedule against the area and R_H at which the cave is expected to become self-propagating. In addition, the coupled model explicitly tracks cave geometry and airgaps. Persistent airgaps introduce uncertainty into draw control and increase the potential for sudden collapse events. In N42, the benefit of preconditioning is therefore twofold: it advances cave initiation and reduces the period during which large, suspended voids persist. In practical terms, that means a more predictable ramp-up and lower exposure to unstable cave geometries.

The practical contribution of the study is the demonstration that a calibrated coupled mechanical flow model can be used not only to explain difficult caving behaviour retrospectively, but also to define actionable thresholds for preconditioning, sequence optimisation and cave-risk mitigation in future sectors.

Acknowledgement

The authors would like to thank Codelco for allowing publication of this paper.

Use of artificial intelligence disclosure statement

In the preparation of this work, the authors used ChatGPT 5.4 for general assistance with writing and editing. The authors have reviewed the content and edited it where required and take full responsibility for said content.

References

Ghazvinian, E, Garza-Cruz, T, Bouzeran, L, Fuenzalida, M, Cheng, Z, Cancino, C & Pierce, M 2020, 'Theory and Implementation of the Itasca Constitutive Model for Advanced Strain Softening (IMASS)', *MassMin 2020: Proceedings, Eighth International Conference & Exhibition on Mass Mining*, pp. 451–461, University of Chile, Santiago.

Hoek, E, Carranza-Torres, C & Corkum, B 2002, 'Hoek-Brown failure criterion - 2002 edition', in R Hammah, W Bawden, J Curran & M Telesnicki (eds), *NARMS-TAC 2002: Mining and Tunnelling Innovation and Opportunity*, vol. 1, pp. 267–273, University of Toronto Press, Toronto.

ITASCA 2023, *FLAC3D - Fast Lagrangian Analysis of Continua in Three-Dimensions*, version 9.0, computer software.

ITASCA 2025, *MASSFLOW - Analysis of Material Flow to Drawpoints*, computer software.

Lorig, LJ & Cundall, PA 2000, *A Rapid Gravity Flow Simulator*, Julius Kruttschnitt Mineral Research Centre and Itasca Consulting Group Inc, Brisbane.

Lorig, L & Pierce, M 2000, *Methodology and Guidelines for Numerical Modelling of Undercut and Extraction Level Behaviour in Caving Mines (ICG00-099-6-15)*, report to the International Caving Study, Itasca Consulting Group Inc.

Pierce, ME 2010, *A Model for Gravity Flow of Fragmented Rock in Block Caving Mines*, PhD thesis, The University of Queensland, Brisbane.